IEEE Access
Multidisciplinary | Rapid Review | Open Access Journal

Received January 4, 2017, accepted February 2, 2017, date of publication February 8, 2017, date of current version March 15, 2017.

*Digital Object Identifier 10.1109/ACCESS.2017.2666156*

# Robust Initial Position Estimation of Permanent Magnet Machine With Low Saliency Ratio

**SHIH-CHIN YANG[1], (Member, IEEE), SHENG-MING YANG[2], (Member, IEEE), AND JING-HUI HU[3]**

[1]National Taiwan University, Taipei 10617, Taiwan
[2]National Taipei University of Technology, Taipei 10618, Taiwan
[3]Industrial Technology Research Institute, Hsinchu 31040, Taiwan

Corresponding author: S.-M. Yang (smyang@ntut.edu.tw)

**ABSTRACT** In permanent magnet (PM) machine drives, the initial position is typically estimated based on the machine inductance variation and the flux saturation. The saliency-based method using the voltage signal injection has demonstrated the reliable position estimation for high salient PM machines at initial state. However considering the saliency-based drive on low salient machines, several implementation issues appear due to the low signal-to-noise ratio of position dependent signals. This paper addresses the implementation issues on saliency-based initial position estimation. It is shown that conventional saliency-based estimation methods might not be able to obtain the correct rotor position on low salient machines due to secondary saliency harmonics. A two-step estimation process is proposed to improve the initial position estimation accuracy on low salient PM machines. Two PM machines with different saliency ratios are tested for the experimental evaluation.

**INDEX TERMS** Machine drives, position sensorless drive, saliency-based drive and high frequency signal injection.

## I. INTRODUCTION

During the machine initial startup, the knowledge of actual rotor positon is essential for the field oriented control (FOC) to maximize the torque density and drive efficiency. Considering the PM machine drive, not only the rotor position but also the magnet polarity needs to detect at initial state [1]–[3]. This technology is referred as the PM machine initial position detection which can be applied for both the position sensorless drive and low resolution sensor-based drive for the initial startup [4], [5].

The machine initial positon can be found by either the rotor alignment to the desired location or the direct position estimation, as seen in Fig. 1. For white good applications, the rotor alignment by applying the DC voltage or current is widely used since the operating loads are not demanded at initial state [6]–[8]. However, the rotor movement and the vibration induce in the system, which might not be accepted for some applications in the silent environment [9].

Instead of rotor alignment, the position can be directly estimated using the spatial signal in a machine. The machine spatial signal is typically induced by the rotor asymmetry (saliency) or the position dependent flux saturation [10]–[15]. However, it is noted that the signal-to-noise ratio (SNR) of these spatial signals are typically low in standard PM machines [16], [17]. To obtain an accurate initial position, several voltage injection methods are developed to excite the spatial signal without the rotor alignment, e.g. persistent high-frequency (HF) voltage [18], [19] or voltage pulses [5], [20] in Fig. 1.

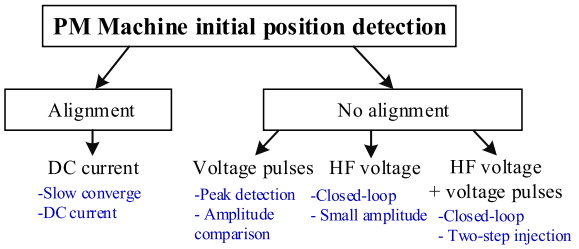


**FIGURE 1.** Illustration of different initial position estimation methods.

Considering the voltage pulse method, a couple of pulses are injected at different estimated positions to induce short-period currents. Because of the rotor asymmetry or flux saturation in a machine, the magnitudes of injection induced currents might be different. By comparing these current magnitudes, the initial rotor position can be identified. It is noted

that the estimation resolution is dependent on the number of voltage pulses. For example, a resolution of ±15° is limited if only six voltage pulses are injected for the position estimation [21]. By increasing the pulses to 21 [22], ±3.8° resolution is resulted with the detection time of 1.7-ms. In general, the estimation accuracy increases as the number of pulses increases. The increased detection time and injection induced vibration are primary limitations of voltage pulse methods on the initial position estimation [23].

A better initial position estimation accuracy has been demonstrated by applying the HF voltage injection method [24], [25]. On the basis, the injection induced HF current contains the position dependent signal which can be isolated for real-time rotor position estimation [26], [27]. Due to the progress of microcontroller, the closed-loop position estimation performance is achieved once the voltage signal is persistently injected. For PM machines with the magnet polarity, an additional polarity dependent current signal is also induced by different saturation conditions between the north pole and south pole [25], [28]–[30]. However, the magnitude of polarity signal is sufficient low comparing to the signal used for the position estimation. As reported in [31], [32], the current measurement offset and inverter harmonics are two limitations for the initial position estimation on low salient PM machines using HF voltage injection.

To overcome the low polarity signal induced by the HF voltage, the pulse injection can integrate to the HF voltage to develop a two-step position estimation process. At the first step, the HF voltage is injected to estimate the rotor position without the correction of magnet polarity. After that, voltage pulses instead of HF voltage are used to determine the polarity as the second step. In [33], two voltage pulses are injected after the HF voltage to improve the polarity detection accuracy on PM machines. [34] superimposes additional q-axis voltages for the polarity detection by comparing the corresponding current responses under different voltage magnitudes. It is important to note that these methods all focus on the improvement of the polarity detection on saliency-based methods. For low salient machines, not only the low polarity signal, but also secondary harmonics in saliency reflected spatial signals need to consider during the initial position estimation process [31].

This paper aims to improve the initial position estimation performance on the saliency-based PM machine drive. It is shown that the saliency-based drive might result in the incorrect initial position estimation on low salient PM machines due to the $4^{th}$-order secondary saliency harmonic. A two-step position estimation process is proposed to minimize the influence of secondary saliency harmonics on the saliency-based drive. At first step, HF voltage is injected to obtain the rotor position. Considering the low magnitude of saliency spatial signal, the estimated position might lead to considerable errors when the initial positon is located near 90° and 270°. To compensate this error, the refinement process is proposed at second step. Four voltage pulses with different magnitudes are injected to improve the estimation accuracy once the estimated position is near these two locations. The saliency-based position estimation performance on low salient PM machines can be improved by adding four voltage pulses at initial state. Two PM machines with different saliency ratios are tested for the experimental evaluation.

## II. SALIENCY-BASED INITIAL POSITION ESTIMATION

This section explains the conventional saliency-based initial position estimation. For the machine drive at initial state, the rotor position can be estimated based on the rotor asymmetry and flux saturation with the injection of HF voltage. Among several injection voltage signals [33]–[37], the square-wave HF voltage has demonstrated the widest position estimation bandwidth on the PM machine sensorless drive [36]. As a result, the square-wave voltage is selected in this paper for the analysis of the saliency-based positon estimation on low salient machines.

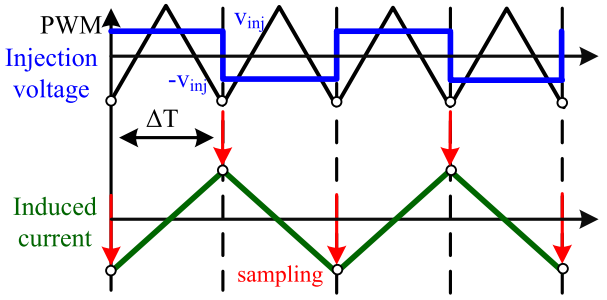


**FIGURE 2.** Relationship between the injected square-wave voltage and pulse width modulation pattern.

On the basis, the HF square-wave voltage can be generated based on the inverter pulse width modulation (PWM), as shown in Fig. 2. For FOC drive, the phase current is typically symmetrically sampled on the bottom of PWM triangular comparator to avoid PWM ripples on current signals. Considering this PWM control strategy, the maximum frequency of square-wave voltage can increase to half of PWM frequency to achieve the widest estimation performance.

In general, the machine model in the rotor referred synchronous frame can be shown by (1) under the small signal assumption of HF voltage.

$$\begin{aligned}\begin{bmatrix} v_d^e \\ v_q^e \end{bmatrix} &= \begin{bmatrix} R_s+pL_d & \omega_e L_d \\ -\omega_e L_q & R_s+pL_q \end{bmatrix}\begin{bmatrix} i_d^e \\ i_q^e \end{bmatrix} + \begin{bmatrix} 0 \\ \omega_e \lambda_{pm} \end{bmatrix} \\ &\approx \begin{bmatrix} pL_d & 0 \\ 0 & pL_q \end{bmatrix}\begin{bmatrix} i_d^e \\ i_q^e \end{bmatrix} \\ &= p\begin{bmatrix} (\Sigma L - \Delta L) & 0 \\ 0 & (\Sigma L + \Delta L) \end{bmatrix}\begin{bmatrix} i_d^e \\ i_q^e \end{bmatrix} \end{aligned} \quad (1)$$

where the subscript dq represents the complex vector in dq coordinate and the superscript e represents the actual rotor frame. $v_d^e$, $v_q^e$ and $i_d^e$, $i_q^e$ are respectively dq voltages and currents, $L_d$ and $L_q$ are d- and q-axis inductance, $\Sigma L$ and $\Delta L$ are average and difference inductance, $R_s$, $\omega_e$ and $\lambda_{pm}$ are

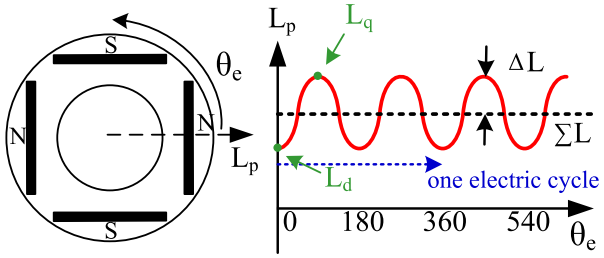


**FIGURE 3.** Illustration of the phase inductance versus the rotor position in the interior PM machine.

the phase resistance, speed and magnet flux, and p is the differential operator. For PM machines, the rotor asymmetry or flux saturation results in the position dependent variation in the inductance. Fig. 3 shows the phase inductance, $L_p$, with respect to the rotor position in an interior PM (IPM) machine. Due to the interior magnet rotor, a $2\theta_e$ spatial harmonic appears where the magnitude is proportional to $\Delta L$. It is noted that in this paper, the inductance variation is modelled by the average inductance $\Sigma L$ and difference inductance $\Delta L$ instead of dq inductances, $L_d$ and $L_q$, to clearly show the influence of secondary spatial harmonics on the saliency-based position estimation. For low salient machines, e.g. surface PM (SPM) machines, $\Delta L$ induced by the saturation is sufficient low which might not be a constant similar to that in Fig. 3 [31]. Under this effect, $\Sigma L/\Delta L$ is selected as inductance variables for the analysis of position estimation on low salient machines.

By superimposing the HF voltage, the impedance voltage drops are dominate, as simplified in (1). The saliency spatial signal can be estimated based on the relationship between HF voltage and current. For the selection of injection voltages, the square-wave voltage in (2) can be injected in the estimated d-axis to extract the saliency spatial signal in HF current.

$$\begin{bmatrix} v_d^{e'} \\ v_q^{e'} \end{bmatrix} = \begin{bmatrix} \pm v_{inj} \\ 0 \end{bmatrix} \tag{2}$$

where $v_{inj}$ is the voltage magnitude and the superscript e' denotes the estimated rotor frame. Assuming that the actual position is unknown at initial state, there is a position error, $\theta_{err} = \theta_e - \hat{\theta}_e$, between the actual rotor frame and the estimated frame. The HF model in the estimated frame can be derived by (3) from the modification of (1).

$$\begin{aligned} &\begin{bmatrix} v_d^{e'} \\ v_q^{e'} \end{bmatrix} \\ &= p\begin{bmatrix} (\Sigma L-\Delta L)\cos\left[2(\theta_e-\hat{\theta}_e)\right] & -\Delta L\sin\left[2(\theta_e-\hat{\theta}_e)\right] \\ -\Delta L\sin\left[2(\theta_e-\hat{\theta}_e)\right] & (\Sigma L+\Delta L)\cos\left[2(\theta_e-\hat{\theta}_e)\right] \end{bmatrix} \\ &\quad\times\begin{bmatrix} i_d^{e'} \\ i_q^{e'} \end{bmatrix} \\ &= p\begin{bmatrix} (\Sigma L-\Delta L)\cos(2\theta_{err}) & -\Delta L\sin(2\theta_{err}) \\ -\Delta L\sin(2\theta_{err}) & (\Sigma L+\Delta L)\cos(2\theta_{err}) \end{bmatrix}\begin{bmatrix} i_d^{e} \\ i_q^{e} \end{bmatrix} \end{aligned} \tag{3}$$

As seen in (3), a $2\theta_{err}$ position dependent harmonic is induced if the estimated e' frame is not aligned with the actual e frame. By superimposing the HF voltage in (2), the injection induced current is shown to be

$$\begin{aligned} &\begin{bmatrix} \Delta i_d^{e'} \\ \Delta i_q^{e'} \end{bmatrix} \\ &= \Delta T\begin{bmatrix} (\Sigma L-\Delta L)\cos(2\theta_{err}) & -\Delta L\sin(2\theta_{err}) \\ -\Delta L\sin(2\theta_{err}) & (\Sigma L+\Delta L)\cos(2\theta_{err}) \end{bmatrix}^{-1} \\ &\quad\times\begin{bmatrix} v_{inj} \\ 0 \end{bmatrix} \\ &= \Delta T\frac{\pm v_{inj}}{\Sigma L^2-\Delta L^2}\begin{bmatrix} (\Sigma L+\Delta L)\cos(2\theta_{err}) \\ \Delta L\sin(2\theta_{err}) \end{bmatrix} \end{aligned} \tag{4}$$

In (4), the current differentiation, $dI_{dq}^{e'}/dt$, is assumed equal to current difference $\Delta I_{dq}^{e'}/\Delta T$ considering the square-wave voltage period, T in Fig. 2, is sufficient small. In addition, $\Delta I_{dq}^{e'}$ in (4) can be obtained by

$$\Delta I_{dq}^{e'} = I_{dq\_T_2}^{e'} - I_{dq\_T_1}^{e'} \tag{5}$$

where $T_2$ and $T_1$ represent the current and last step of $\Delta I_{dq}^{e'}$. For the saliency-based method, the rotor position is estimated by manipulating $2\theta_{err}$ to be zero. It is noted that a $\pm$ sign appears in $\Delta I_{dq}^{e'}$ due to the modulation of square-wave voltage. This $\pm$ sign can be removed by (6).

$$\begin{aligned} \begin{bmatrix} \Delta i_{d\_err} \\ \Delta i_{q\_err} \end{bmatrix} &= \text{sign}(\pm v_{inj}) \times \begin{bmatrix} \Delta i_d^{e'} \\ \Delta i_q^{e'} \end{bmatrix} \\ &= \frac{\Delta T v_{inj}}{\Sigma L^2-\Delta L^2}\begin{bmatrix} (\Sigma L+\Delta L)\cos(2\theta_{err}) \\ \Delta L\sin(2\theta_{err}) \end{bmatrix} \end{aligned} \tag{6}$$

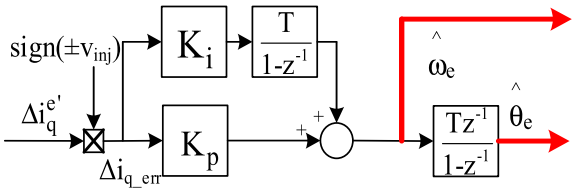


**FIGURE 4.** Position and speed estimation based on the saliency signal $\Delta i_q^{e'}$.

Fig. 4 illustrates the position and speed estimation, $\hat{\theta}_e$ and $\hat{\omega}_e$, based on the phase-locked loop (PLL). The PLL estimation bandwidth can be designed from the selection of controller gains, $K_p$ and $K_i$. For PLL to be locally stable, the closed-loop system with the negative feedback must result where $\sin(2\theta_{err}) > 0$ once $\theta_{err} > 0$ or $\sin(2\theta_{err}) < 0$ once $\theta_{err} < 0$. Fig. 5 shows the waveform of $\sin(2\theta_{err})$ versus $\theta_{err}$. Due to the nonlinearity of $\sin(2\theta_{err})$, the stable PLL can only be maintained when $-45° < \theta_{err} < 45°$, $135° < \theta_{err} < 180°$, and $-180° < \theta_{err} < -135°$. In order to analyze the nonlinear PLL property in Fig. 4, it is worth to apply the partial derivative on $\sin(2\theta_{err})$ to linearize the nonlinear quantity, as seen

in (7).

$$\left.\frac{\partial \Delta i_{q\_err}}{\partial \theta_e}\right|_{\substack{\theta_e=\theta_{e0}\\ \hat{\theta}_e=\hat{\theta}_{e0}}} = \left.\frac{\Delta L \Delta T v_{inj}}{\Sigma L^2 - \Delta L^2} 2\cos\left(2\theta_e - 2\hat{\theta}_e\right)\right|_{\substack{\theta_e=\theta_{e0}\\ \hat{\theta}_e=\hat{\theta}_{e0}}} = k_{sal} 2\cos\left(2\theta_{e0} - 2\hat{\theta}_{e0}\right) \quad (7)$$

where $k_{sal}$ is defined as the magnitude of saliency signal to simplify the following analysis, and $\theta_{e0}$ and $\hat{\theta}_{e0}$ represent the operating points of PLL.

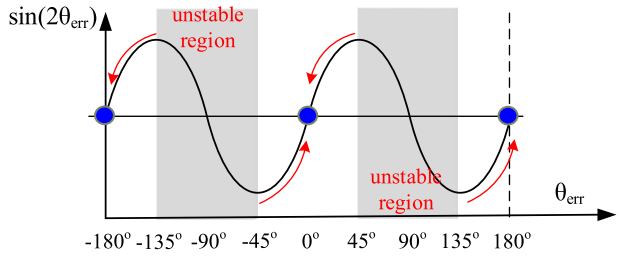


**FIGURE 5.** Stability analysis of the PLL in Fig. 4.

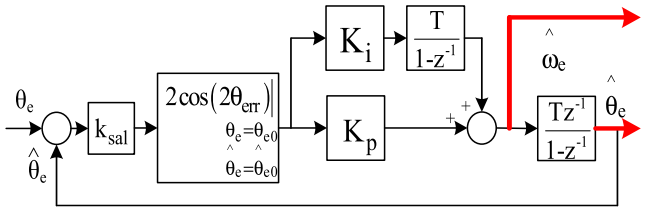


**FIGURE 6.** Linearization of PLL with the operating point $\theta_{err} = \theta_{err\_0}$.

Fig. 6 shows the signal flowchart for the linearized PLL. For the operating points at unstable regions in Fig. 5, e.g. $\theta_{err0}$ =90° if $\theta_{e0} = 90°$ and $\hat{\theta}_{e0} = 0°$, the positive feedback is observed. Under this effect, $\theta_{err0}$ quickly diverges to stable regions depicted in Fig. 5. At steady state, $\theta_{err}$ eventually converges to 0° or 180°. Considering $\theta_{err} = 180°$, additional polarity correction is required for PM machines because $\hat{\theta}_{e0}$ is not actually equal to $\theta_{e0}$ but with the error of 180°. In addition for low salient machines, the low SNR due to the secondary harmonics results in the incorrect estimation on $\hat{\theta}_e$. Thus, implementation issues need to consider for the initial position estimation using the saliency signal with low SNR.

## III. TWO-STEP INITIAL POSITION ESTIMATION

This section proposes a two-step position estimation process to improve the saliency-based initial position estimation on low salient machines. The influence of secondary harmonics on the saliency-based position estimation is firstly explained. The refinement process based on the voltage pulse injection is then developed to improve the estimation accuracy.

### A. SECONDARY SALIENCY HARMONICS

For low salient machines e.g. SPM machines, the saliency is primary induced by the flux saturation. Instead of $2\theta_e$ harmonic in Fig. 3, the inductance contains secondary harmonics, such as $4\theta_e$, $6\theta_e$, $8\theta_e$ harmonic etc.. It is noted that $4\theta_e$ harmonic is the dominant secondary harmonic, as reported in [31]. Considering the $4\theta_e$ harmonic, the partial derivative of nonlinear PLL in (7) should be modified by

$$\begin{aligned}\left.\frac{\partial \Delta i_{q\_err}}{\partial \theta_e}\right|_{\substack{\theta_e=\theta_{e0}\\ \hat{\theta}_e=\hat{\theta}_{e0}}} &= \left.\frac{\partial}{\partial \theta_e}\left[k_{sal}\sin\left(2\theta_{err}\right) + k_{sal4}\sin\left(2\theta_{err} + 2\theta_e\right)\right]\right|_{\substack{\theta_e=\theta_{e0}\\ \hat{\theta}_e=\hat{\theta}_{e0}}}\\ &= \left.\frac{\partial}{\partial \theta_e}\left[k_{sal}\sin\left(2\theta_e - 2\hat{\theta}_e\right) + k_{sal4}\sin\left(4\theta_e - 2\hat{\theta}_e\right)\right]\right|_{\substack{\theta_e=\theta_{e0}\\ \hat{\theta}_e=\hat{\theta}_{e0}}}\\ &= \left.\left[k_{sal}2\cos\left(2\theta_{e0} - 2\hat{\theta}_{e0}\right) + k_{sal4}4\cos\left(4\theta_{e0} - 2\hat{\theta}_{e0}\right)\right]\right|_{\substack{\theta_e=\theta_{e0}\\ \hat{\theta}_e=\hat{\theta}_{e0}}}\end{aligned} \quad (8)$$

where $k_{sal4}$ is the magnitude of $4\theta_e$ saliency harmonic which is shown to be

$$k_{sal4} = \frac{\Delta L_4 \Delta T v_{inj}}{\Sigma L^2 - \Delta L_4^2} \quad (9)$$

In (9), $\Delta L_4$ represents the difference inductance with respect to $4\theta_e$ harmonic. As seen in (8), $4\theta_e$ harmonic results in the constant position error on the estimated $\hat{\theta}_e$. Fig. 7 and 8 simulates 3-D plot of $\Delta i_{q\_err}$ in (7) and (8) versus $\theta_{err}$ at different initial position $\theta_e$. In Fig. 7 under the condition of the saliency-based estimation without secondary saliency harmonics, the waveforms of $\Delta i_{q\_err}$ versus $\theta_{err}$ are the same at different $\theta_e$. In this case, the estimated $\hat{\theta}_e$ can always converge to either 0° or 180° at any initial positions.

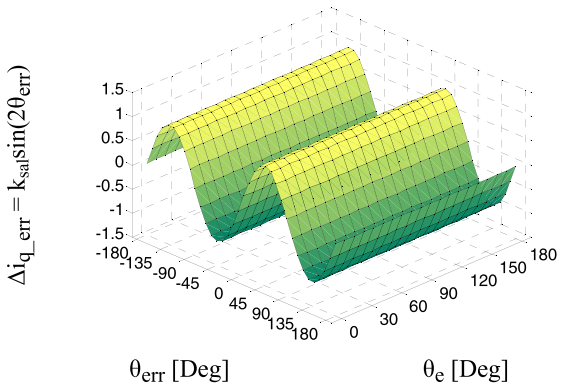


**FIGURE 7.** Simulation of $k_{sal}\sin(2\theta_{err})$ versus $\theta_{err}$ at different initial rotor position $\theta_e$ ($k_{sal} = 1$ and no secondary saliency harmonic).

By contrast, Fig. 8 shows $\Delta i_{q\_err}$ versus $\theta_{err}$ at different $\theta_e$ when $4\theta_e$ harmonic is included in the saliency signal, $\Delta i_{q\_err}$. In this case, $k_{sal4}$ is equal to $0.5k_{sal}$ in (8) to simulate the condition where the magnitude of $4\theta_e$ saliency harmonic is

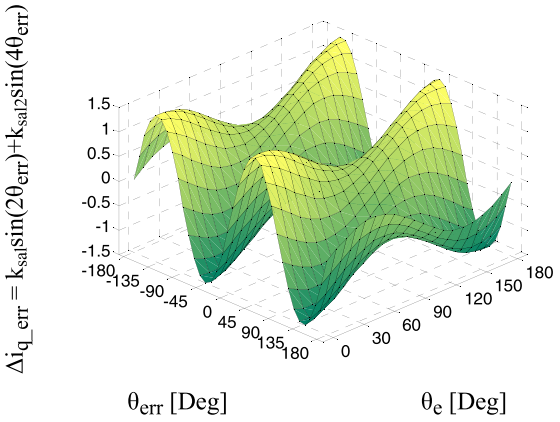


**FIGURE 8.** Simulation of $k_{sal}\sin(2\theta_{err}) + k_{sal2}\sin(4\theta_{err})$ versus $\theta_{err}$ at different initial rotor position $\theta_e$($k_{sal} = 1$ and $k_{sal2} = 0.5$ on $4\theta_e$ secondary saliency harmonic).

equal to that of $2\theta_e$ harmonic. It is found that the waveforms of $\Delta i_{q\_err}$ versus $\theta_{err}$ change with respect to different initial positions, $\theta_e$. When $\theta_e$ is at 22.5°, not error appears on $\hat{\theta}_e$ though the saliency signal contains $4\theta_e$ harmonic, as verified by the model in (8). However, the estimation error increases once $\theta_e$ increases or decreases from 22.5°. The peak error is induced when $\theta_e$ is located at 90° or 270°, as seen for $\Delta i_{q\_err}$ in Fig. 8. Once 90° error induces in estimated $\hat{\theta}_e$, no electromagnetic torque can generate based on FOC.

### *B. TWO-STEP INITIAL POSITION ESTIMATION*

To improve the degraded saliency-based estimation on low salient machines, a two-step initial position process is proposed to minimize the influence of $4\theta_e$ harmonic on the initial position estimation. Fig. 9 illustrates the proposed two-step initial position estimation process. At first step, the HF square-wave voltage is injected to obtain the estimated $\hat{\theta}_e$ based on the PLL developed in Fig. 6. Considering the $4\theta_e$ harmonic, the peak position error of 90° appears when $\theta_e$ is located at 90° or 270°. The resulting estimated $\hat{\theta}_e$ should be either 0° or 180°, leading to zero torque production. It is important to note that when $\hat{\theta}_e$ is located near 0° or 180°, additional voltage pulses can be injected to correct the estimation error as the second step. Fig. 10 simulates the inductance versus the rotor position considering the $4\theta_e$ harmonic in a machine. It is found that d-axis inductance (at $\theta_e = 0°$) is still lower than the q-axis inductance ($\theta_e = 90°$) under the same condition in Fig. 8 used for the saliency-based position estimation. Although $4\theta_e$ harmonic results in the considerable 90° error on the saliency-based method, this error is able to correct based on the pulses injection method.

The proposed $\hat{\theta}_e$ correction is illustrated at second step in Fig. 9. It is noted that $\hat{\theta}_e$ correction is only applied when $-5° < \hat{\theta}_e < 5°$ and $175° < \hat{\theta}_e < 185°$ considering the peak saliency-based estimation error without the torque production. Once $\hat{\theta}_e$ is initially located near these two positions, two voltage pulses, $V_{1d\_pulse\_pos}$ and $V_{1q\_pulse\_pos}$,

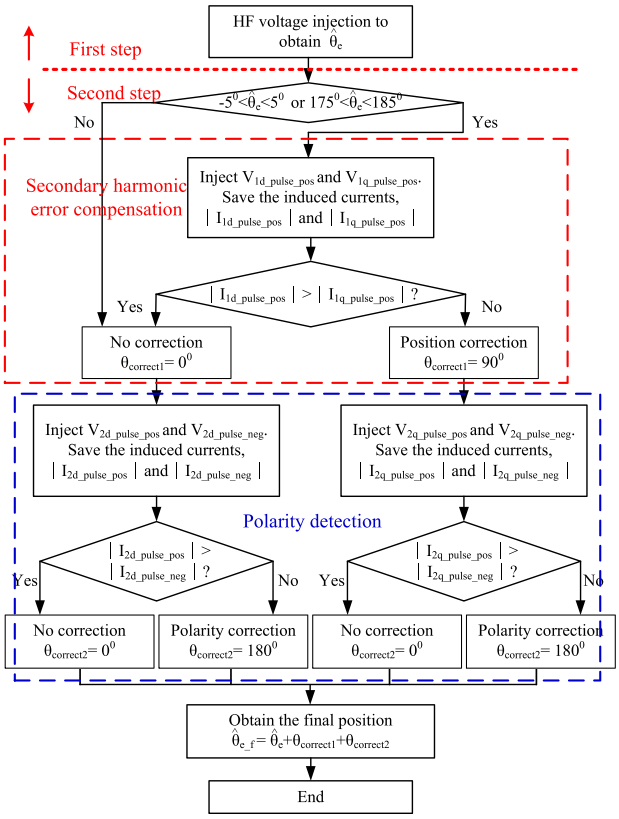


**FIGURE 9.** Proposed two-step initial position estimation process for low salient machines.

are respectively injected at estimated d-axis ($\hat{\theta}_e = 0°$) and q-axis ($\hat{\theta}_e = 90°$) to compare the corresponding injection induced currents, $I_{1d\_pulse\_pos}$ and $I_{1q\_pulse\_pos}$. As shown for the inductance distribution in Fig. 10, $|I_{1d\_pulse\_pos}|$ should be higher than $|I_{1q\_pulse\_pos}|$ if $\hat{\theta}_e$ is located near 0° and 180°. However, once a 90° error occurs, $|I_{1d\_pulse\_pos}|$ would be smaller than $|I_{1q\_pulse\_pos}|$ as illustrated in Fig. 10. At this condition, a correction angle, $\theta_{correct1} = 90°$, is applied to resolve the saliency-based estimation error resulting from $4\theta_e$ secondary harmonic which is depicted by the red box in Fig. 9.

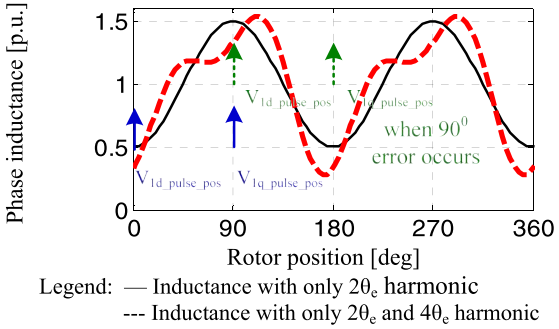


**FIGURE 10.** Inductance versus rotor position considering secondary saliency harmonics (1 p.u, $2\theta_e$ saliency harmonic and 0.5 p.u. $4\theta_e$ saliency harmonic).

### C. POLARITY IDENTIFICATION AT INITIAL STATE

For PM machines, not only the rotor position but also the polarity must be identified at initial state. For low salient machines, the polarity detection based on the saturation signal induced by the HF voltage injection might result in the incorrect polarity detection due to the current measurement offset and inverter dead-time harmonics [31].

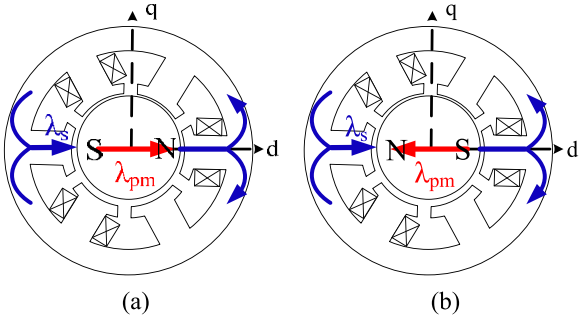


**FIGURE 11.** Interaction between the magnet flux and winding flux (a) augment the overall flux making stator into saturation, or (b) subtract from the flux making stator away from saturation.

In this paper instead of HF voltage injection, the pulse injection method is implemented to obtain the polarity in PM machines. On the basis, the polarity is identified based on the flux saturation. Fig. 11 compares the stator flux operation at the direction of (a) north pole and (b) south pole. As seen in Fig. 11(a), the overall stator flux is augmented once the winding flux, $\lambda_w$, is on the same direction with respect to the magnet flux, $\lambda_{pm}$. The overall stator flux becomes $\lambda_{pm} + \lambda_w$, leading to the inductance falls into the saturation. By contrast in (b), the overall stator flux is subtracted when $\lambda_w$ is on the opposite direction to $\lambda_{pm}$. The inductance leaves from the saturation area.

The proposed polarity detection is illustrated by the blue box in Fig. 9. Two more voltage pulses, $V_{2dq\_pulse\_pos}$ and $V_{2dq\_pulse\_neg}$, with different polarities are respectively injected in the estimated d-axis. The magnet polarity is identified by comparing the magnitudes of injection induced currents, $I_{2dq\_pulse\_pos}$ and $I_{2dq\_pulse\_neg}$. As shown in Fig. 12(a) when the rotor position is located in the north pole area, the resulting injection current $|I_{2dq\_pulse\_pos}|$ is higher than $|I_{2dq\_pulse\_neg}|$ because the injection of $V_{2dq\_pulse\_pos}$ results in more inductance saturation. By contrast in (b) when the position is in the south pole, $|I_{2dq\_pulse\_pos}|$ is lower than $|I_{2dq\_pulse\_neg}|$ due to the reduced saturation resulting from the injection of $V_{2dq\_pulse\_pos}$. As see in Fig. 9, a correction angle, $\theta_{correct2} = 180°$, can be determined to correct the polarity once $|I_{2dq\_pulse\_pos}| < |I_{2dq\_pulse\_neg}|$. After the two-step estimation process, the final initial rotor position, $\hat{\theta}_{e\_f}$, is obtained by

$$\hat{\theta}_{e\_f} = \hat{\theta}_e + \theta_{correct1} + \theta_{correct2} \tag{10}$$

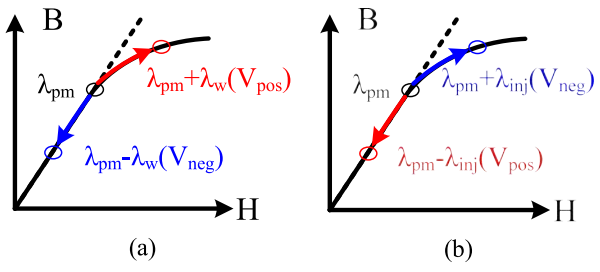


**FIGURE 12.** Stator flux operation with the influence of voltage pulses at the area of a) north pole and (b) south pole.

## IV. EXPERIMENTAL RESULTS

Two types of PM machines are experimentally tested in this section to evaluate the proposed two-step initial positon estimation performance. They are a 364-W high-salient IPM machine and a 180-W low-salient SPM machine. An inverter with six insulated-gate bipolar transistors (IGBT) switches is used to drive these two machines. Because the power levels on these two machines are relatively small, pulse-wide-modulation (PWM) frequency is increased to 18-kHz in order to achieve a 9-kHz square-wave voltage injection frequency for the high bandwidth saliency-based position estimation. Inverter dead-time is set at 1-$\mu$s equal to 0.56-% PWM duty cycle. The DC bus voltage of 150-V is used to drive these two machines. All the drive and position estimation algorithms are implemented in a 32-bit microcontroller, TI-TMS320F28335.

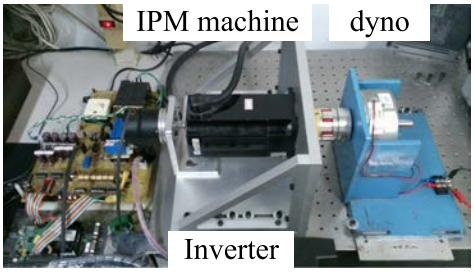


**FIGURE 13.** IPM machine test bench for the initial position estimation.

### A. IPM MACHINE POSITION ESTIMATION

A 364-W 4-pole IPM machine is firstly tested for the evaluation of proposed two-step initial position estimation. The machine test setup is shown in Fig. 13. Key machine parameters are listed in Table 1. The corresponding saliency ratio ($L_q/L_d$) is 1.41 based on the RLC meter measurement.

**TABLE 1.** Tested IPM machine characteristics.

| Characteristics | Values |
|---|---|
| Rotor poles | 4-pole |
| Rated torque | 0.58-Nm |
| Rated current | 2-A |
| Rated speed | 6000-rpm |
| Resistance | 1.15-Ω |
| Inductance | 4.6-mH($L_d$)/6.5-mH($L_q$) |
| DC bus voltage | 150-V |

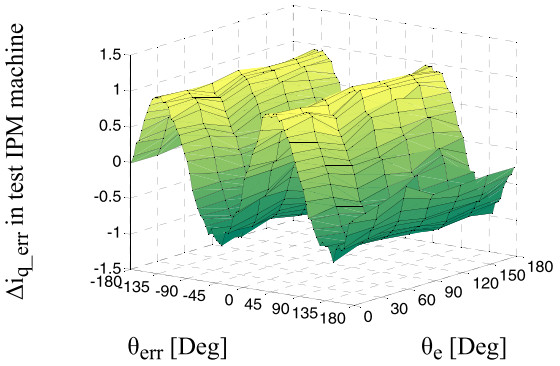


**FIGURE 14.** Experiment of normalized $\Delta i_{q\_err}$ versus $\theta_{err}$ at different initial rotor position $\theta_e$ in the IPM machine (locked-rotor test).

Fig. 14 shows the measured $\Delta i_{q\_err}$ versus $\theta_{err}$ at different initial position, $\theta_e$. In this figure, the IPM machine is locked at different rotor positions from 0° to 180°. The square-wave voltage with the frequency of 9-kHz (half of PWM frequency) is injected at different estimated $\hat{\theta}_e$ where the position error, $\theta_{err} = \theta_e - \hat{\theta}_e$, is manipulated from -180° to 180°. Ideally without the secondary saliency harmonics, $\Delta i_{q\_err}$ should contain only a $2\theta_e$ harmonic at different $\theta_e$ as $\theta_{err}$ varies from -180° to 180°, which is derived in (6). In this IPM machine, the saliency ratio is 1.41 where the machine can be categorized into high-salient machines. As a result, the measured $\Delta i_{q\_err}$ versus $\theta_{err}$ is almost the same to the simulation in Fig. 7 without secondary saliency harmonics.

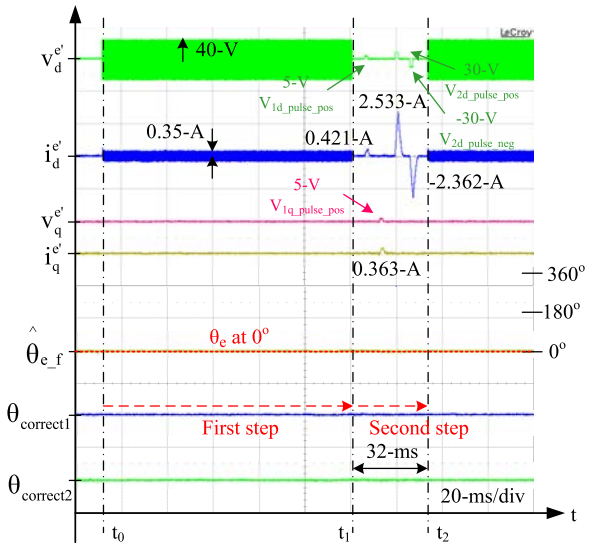


**FIGURE 15.** Two-step initial position estimation performance on the IPM machine when $\hat{\theta}_e$ is initially at 0-deg and actual $\theta_e$ is at 0-deg.

Figs. 15-18 evaluate the proposed two-step initial position estimation on this IPM machine when $\hat{\theta}_e$ is initially at 0° and $\theta_e$ is at 0°, 90°, 180° and 270°. In these four tests, time-domain waveforms of $v_d^{e'}$, $i_d^{e'}$, $v_q^{e'}$, $i_q^{e'}$, $\hat{\theta}_{e\_f}$, $\theta_{correct1}$ and $\theta_{correct2}$ in Fig.9 are respectively shown. During the first step, the saliency-based estimation using the square-wave voltage

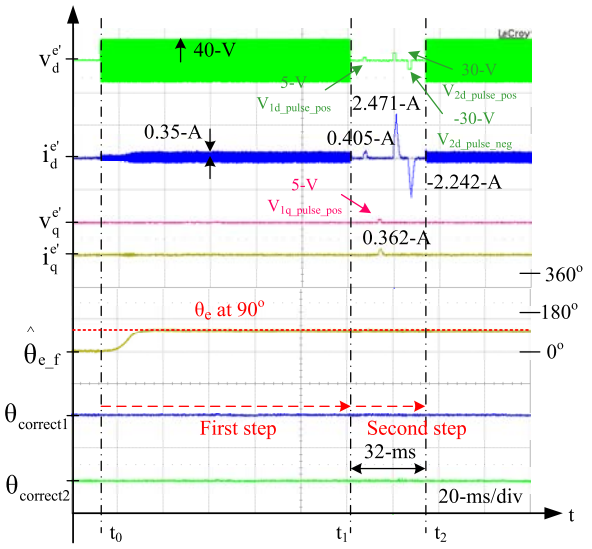


**FIGURE 16.** Two-step initial position estimation performance on the IPM machine when $\hat{\theta}_e$ is initially at 0-deg and actual $\theta_e$ is at 90-deg.

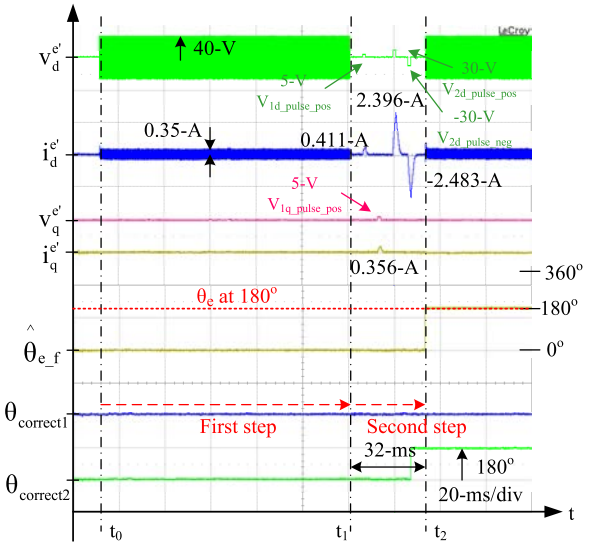


**FIGURE 17.** Two-step initial position estimation performance on the IPM machine when $\hat{\theta}_e$ is initially at 0-deg and actual $\theta_e$ is at 180-deg.

injection in Fig. 4 is applied to obtain the rotor position. The injection voltage magnitude, $v_{inj}$ in (2), is 40-V at 9-kHz. During the second step, four voltage pulses in Fig. 9 are sequentially injected for the secondary harmonic compensation and polarity detection. The pulse voltages are 5-V and 30-V with 1.3-ms period (20 PWM cycles) respectively for the harmonic compensation and polarity detection.

As seen in Fig. 15 when $\theta_e$ is at 0°, the estimated position $\hat{\theta}_{e\_f}$ quickly converges to 0° with the saliency-based position estimation during the first step. Once the estimation process reaches $t_1$, voltage pulses instead of square-wave voltage are injected for the estimation refinement. For the secondary harmonic compensation, two 5-V voltage pulses are injected respectively in the estimated d- and q-axis,

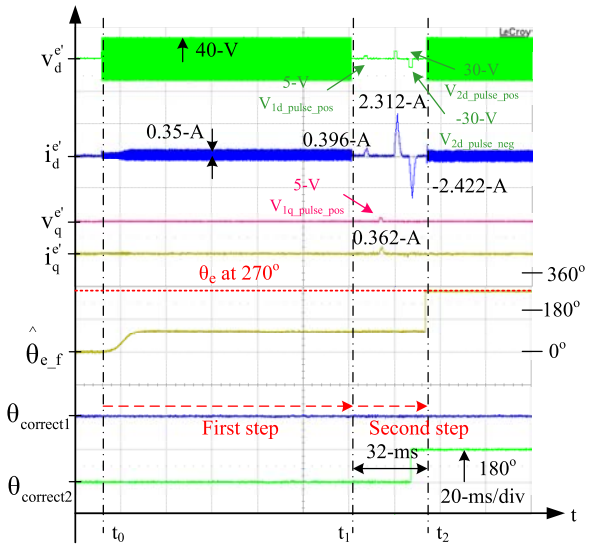


**FIGURE 18.** Two-step initial position estimation performance on the IPM machine when $\hat{\theta}_e$ is initially at 0-deg and actual $\theta_e$ is at 270-deg.

inducing current spikes, $I_{1d\_pulse\_pos}$ and $I_{1q\_pulse\_pos}$. Because $|I_{1q\_pulse\_pos}| < |I_{1d\_pulse\_pos}|$, the estimated $\hat{\theta}_{e\_f}$ is concluded close to the initial position $\theta_e$. Thus, no compensation is required where $\theta_{correct1} = 0°$. In this IPM machine, negligible secondary harmonics are observed in Fig 14 leading to no influence on the harmonic compensation during the second step. By contrast for the polarity detection, two 30-V voltage pulses are also injected in estimated 0° and 180°, resulting in currents spikes, $I_{2dq\_pulse\_pos}$ and $I_{2dq\_pulse\_neg}$. Since $|I_{2dq\_pulse\_pos}| > |I_{2dq\_pulse\_neg}|$, no polarity correction where $\theta_{correct2} = 0°$ is determined. After the two-step estimation, the final estimated position, $\hat{\theta}_{e\_f}$, is obtained by (10) equal to 0°.

Fig. 16 shows the same experiment but $\theta_e$ is changed to 90°. At the beginning of first step, $\hat{\theta}_{e\_f}$ converges to 90° with the saliency-based position estimation. After that, four voltage pulses are injected during the second step. Similar to Fig. 15, no secondary harmonic and polarity compensation where $\theta_{correct1} = \theta_{correct2} = 0°$ is determined. After the two-step estimation, the final estimated position, $\hat{\theta}_{e\_f}$, is obtained by 90° equal to $\theta_e$.

Fig. 17 shows the same experiment but $\theta_e$ is at 180°. During the first step, $\hat{\theta}_{e\_f}$ converges to 0° with 180° error with respect to the actual position. For the saliency-based estimation, the estimated position might converge to another operating point illustrated in Fig. 5 when the error is beyond 180°. This polarity error can be compensated based on the proposed pulses injection during the second step. As seen in Fig. 17, two 30-V voltage pulses are injected in estimated 0° and 180° for the polarity detection. By observing the current spike $|I_{2dq\_pulse\_pos}| < |I_{2dq\_pulse\_neg}|$, $\theta_{correct2} = 180°$ is determined resulting in the final estimated position $\hat{\theta}_{e\_f} = 180°$. After the two-step estimation, the estimated $\hat{\theta}_{e\_f}$ is equal to initial position $\theta_e = 180°$.

Finally, Fig. 18 shows the experiment when $\theta_e$ is at 270°. During the first step, $\hat{\theta}_{e\_f}$ converges to 90° with the saliency-based estimation. Similar to Fig. 17, 180° error occurs due to the limitation on the saliency-based estimation. This polarity error is also compensated based on voltage pulses injection during the second step. The final estimated position $\hat{\theta}_{e\_f} = 270°$ is obtained after the two-step estimation. According to these four experiments, it is concluded that the proposed harmonic compensation has no effect on high salient IPM machines while the polarity error can be compensated by applying two voltage pulses during the second step illustrated in Fig 9.

### B. SPM MACHINE POSITION ESTIMATION

A 180-W 8-pole SPM machine is also tested to verify the two-step estimation performance. Fig. 19 shows a photograph of machine test bench. Machine parameters are listed in Table 2 where the saliency ratio ($L_q/L_d$) is 1.25.

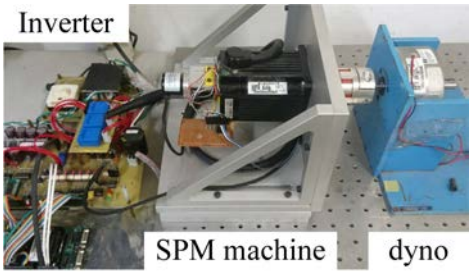


**FIGURE 19.** SPM machine test bench for the initial position estimation.

**TABLE 2.** Test SPM machine characteristics.

| Characteristics | Values |
|---|---|
| Rotor poles | 8-pole |
| Rated torque | 0.57-Nm |
| Rated current | 0.94-A |
| Rated speed | 3000-rpm |
| Resistance | 2.7-Ω |
| Inductance | 7.31-mH($L_d$)/9.15-mH($L_q$) |
| DC bus voltage | 150-V |

Fig. 20 shows $\Delta i_{q\_err}$ versus $\theta_{err}$ at different $\theta_e$. Similar to Fig. 14, the SPM machine is located at different positions from 0° to 180°. The square-wave voltage with the same magnitude and frequency is injected at different $\hat{\theta}_e$ where $\theta_{err}$ is changed from −180° to 180°. In Fig. 18, $\Delta i_{q\_err}$ contains secondary saliency harmonics due to the low saliency in this SPM machine. More importantly, the peak error of $\Delta i_{q\_err}$ versus $\theta_{err}$ appears when $\theta_e$ is at 90°. The minimum error of $\Delta i_{q\_err}$ versus $\theta_{err}$ is approximately located at 30°. This measurement result is similar to the simulation result in Fig. 8 though the magnitude of $k_{sal2}$ in (8) is not exactly equal to $0.5k_{sal}$ in this test machine. Based on this experiment, it is observed that this SPM machine contains considerable secondary harmonics, especially $4\theta_e$ harmonic. The peak position estimation error should induce when the positon $\theta_e$ is initially at 90° to 270°.

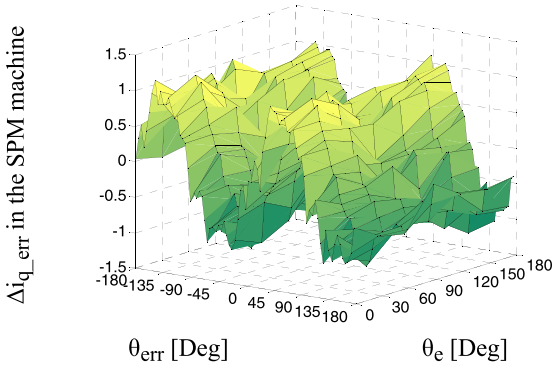


**FIGURE 20.** Experiment of normalized $\Delta i_{q\_err}$ versus $\theta_{err}$ at different initial rotor positions $\theta_e$ in the SPM machine (locked-rotor test).

Similar to the tests in the IPM machine, Figs. 21-24 show the two-step initial positon estimation performance on this SPM machine when $\hat{\theta}_e$ is initially at 0°, 90°, 180° and 270°. During the first step, the saliency-based estimation is applied for the position estimation. Four voltage pulses are then injected during the second step. The square-wave voltage magnitude/frequency and voltage pulses magnitude/duty are same to Figs. 15-18 for the comparison between these two machines.

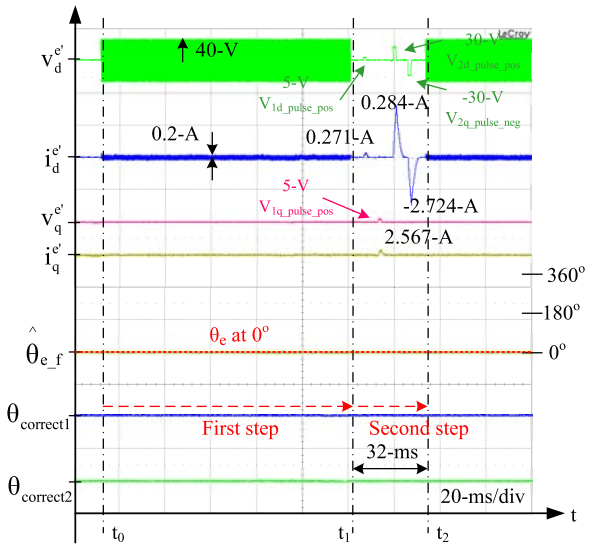


**FIGURE 21.** Two-step initial position estimation performance on the SPM machine when $\hat{\theta}_e$ is initially at 0-deg and actual $\theta_e$ is at 0-deg.

Fig. 21 shows the position estimation experiment when $\theta_e$ is at 0°. Similar to the result in Fig. 15, $\hat{\theta}_{e\_f}$ converges to 0° with the saliency-based estimation during the first step. Four voltage pulses are then injected during the second step. Because $|I_{1q\_pulse\_pos}| < |I_{1d\_pulse\_pos}|$ and $|I_{2dq\_pulse\_pos}| > |I_{2dq\_pulse\_neg}|$, no harmonic and polarity compensation should be applied where $\theta_{correct1} = \theta_{correct2} = 0°$. After the two-step estimation, the final estimated position, $\hat{\theta}_{e\_f}$ is obtained by 0° equal to $\theta_e$.

Fig. 22 shows the position estimation experiment when $\theta_e$ is at 90°. It is noteworthy that 90° is the position where the

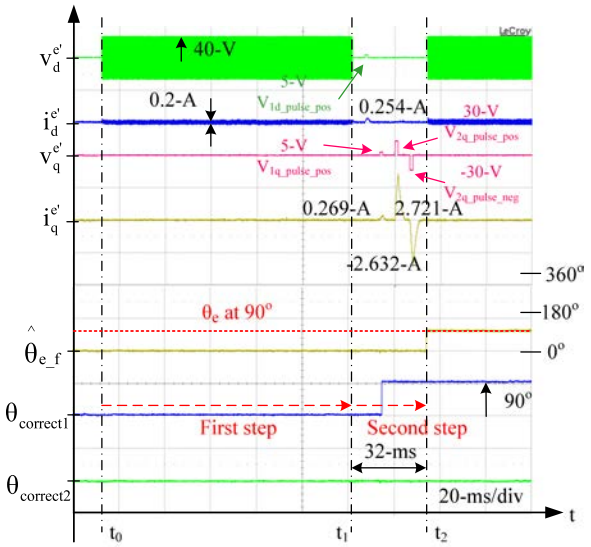


**FIGURE 22.** Two-step initial position estimation performance on the SPM machine when $\hat{\theta}_e$ is initially at 0-deg and actual $\theta_e$ is at 90-deg.

peak saliency-based estimation error might appear according to Fig. 20. Different to the experiment in Fig. 16, $\hat{\theta}_{e\_f}$ converges to 0° during the first step, resulting in 90° position error with respect to $\theta_e$. The $4\theta_e$ saliency harmonic error in the SPM machine illustrated in Fig. 10 is the primary reason to induce this estimation error. However by applying voltage pulses during the second step, this saliency harmonic error is compensated. As seen in Fig, 22, the pulse injection induced current spike $|I_{1q\_pulse\_pos}| > |I_{1d\_pulse\_pos}|$ is demonstrated. According to the inductance waveform in Fig. 10, a 90° estimation error is observed and $\theta_{correct1} = 90°$ is applied to compensate this harmonic error. By contrast for the polarity detection, $\theta_{correct2} = 0°$ is determined because $|I_{2dq\_pulse\_pos}| > |I_{2dq\_pulse\_neg}|$. After the two-step estimation, the final estimated position, $\hat{\theta}_{e\_f}$, can be corrected at 90° equal to $\theta_e$.

Fig. 23 show the experiment when $\theta_e$ is at 180°. Similar to Fig. 17, $\hat{\theta}_{e\_f}$ converges to 0° with 180° position error due to the polarity detection error on the saliency-based estimation. This polarity error is compensated using the voltage pulses injection during the second step. After obtaining the induced current spike $|I_{2dq\_pulse\_pos}| < |I_{2dq\_pulse\_neg}|$ in Fig. 23, $\theta_{correct2} = 180°$ is determined for the polarity error compensation. After the two-step estimation, the estimated $\hat{\theta}_{e\_f}$ is corrected at 180° equal to $\theta_e$.

Fig. 24 shows the experiment when $\theta_e$ is at 270°. As seen from the saliency harmonic waveform in Fig. 20, the peak saliency-based estimation error should occur. In addition, a 180° polarity error also appears with the saliency-based position estimation during the first step. After applying four voltage pulses during the second step, the current spike $|I_{1q\_pulse\_pos}| > |I_{1d\_pulse\_pos}|$ and $|I_{2dq\_pulse\_pos}| < |I_{2dq\_pulse\_neg}|$ are obtained, leading to $\theta_{correct1} = 90°$ and $\theta_{correct2} = 180°$ for the correction on the estimated position.

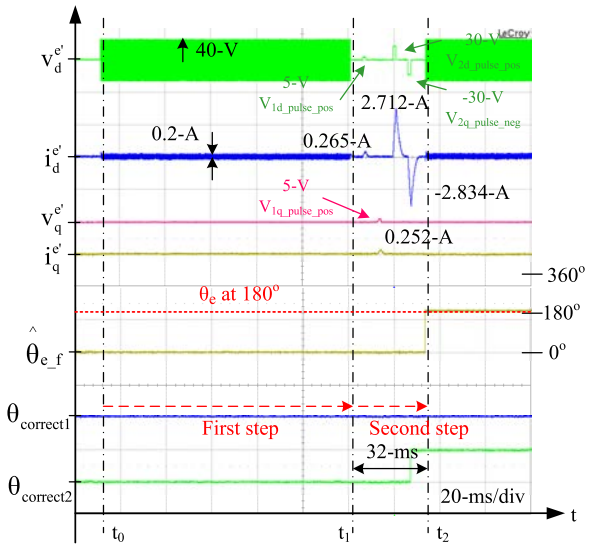


**FIGURE 23.** Two-step initial position estimation performance on the SPM machine when $\hat{\theta}_e$ is initially at 0-deg and actual $\theta_e$ is at 180-deg.

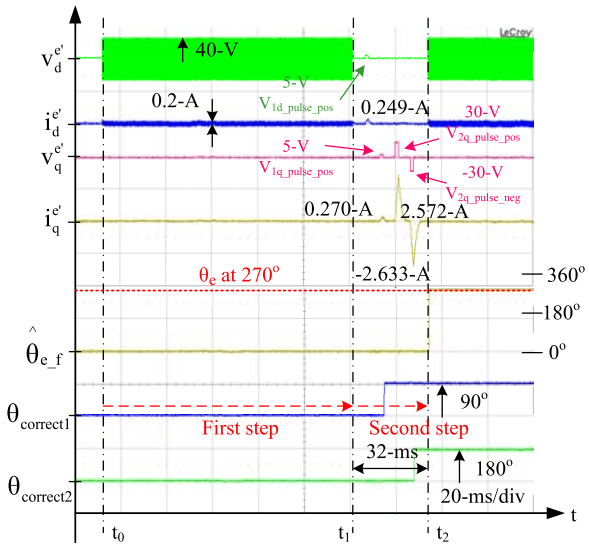


**FIGURE 24.** Two-step initial position estimation performance on the SPM machine when $\hat{\theta}_e$ is initially at 0-deg and actual $\theta_e$ is at 270-deg.

The final estimated $\hat{\theta}_{e\_f}$ is then obtained by 270° equal to $\theta_e$. Based on these four experimental results, it is concluded that the initial position estimation performance is improved on low salient SPM machines by adding voltage pulses in Fig. 9 for both the saliency harmonic and polarity compensation.

## V. CONCLUSIONS

Several conclusions are listed as follows:

- Secondary saliency harmonics might result in considerable position errors on low salient machines using the saliency-based estimation with high frequency voltage injection. Among these secondary harmonics, $4\theta_e$ harmonic is the dominant secondary harmonic, resulting in a peak estimation error of 90° when the rotor positon is initially at 90° or 270°.
- A two-step initial position estimation process is proposed for both the saliency harmonic and polarity compensation. By adding four voltage pulses after the saliency-based estimation, the secondary harmonic error and magnet polarity error can be compensated, leading to an improved initial position estimation performance.
- For high salient IPM machines, the influence of secondary saliency harmonic on the initial position estimation is negligible according to experimental results. However, the magnet polarity still needs to correct on the saliency-based position estimation.
- For low salient SPM machines, a considerable $4\theta_e$ secondary saliency harmonic is observed instead of $2\theta_e$ primary saliency harmonic. By applying the proposed two-step initial position estimation using voltage pulses during the second step, this type of position error can be corrected when the initial position is near 90° or 270°.

## REFERENCES

[1] N. Matsui, "Sensorless PM brushless DC motor drives," *IEEE Trans. Ind. Electron.*, vol. 43, no. 2, pp. 300–308, Apr. 1996.
[2] A. Consoli, G. Scarcella, and A. Testa, "Industry application of zero-speed sensorless control techniques for PM synchronous motors," *IEEE Trans. Ind. Appl.*, vol. 37, no. 2, pp. 513–521, Mar. 2001.
[3] E. Robeischl and M. Schroedl, "Optimized INFORM measurement sequence for sensorless PM synchronous motor drives with respect to minimum current distortion," *IEEE Trans. Ind. Appl.*, vol. 40, no. 2, pp. 591–598, Mar. 2004.
[4] F. Betin *et al.*, "Trends in electrical machines control: Samples for classical, sensorless, and fault-tolerant techniques," *IEEE Ind. Electron. Mag.*, vol. 8, no. 2, pp. 43–55, Jun. 2014.
[5] J. Holtz, "Acquisition of position error and magnet polarity for sensorless control of PM synchronous machines," *IEEE Trans. Ind. Appl.*, vol. 44, no. 4, pp. 1172–1180, Jul. 2008.
[6] Z. Wang, K. Lu, and F. Blaabjerg, "A simple startup strategy based on current regulation for back-EMF-based sensorless control of PMSM," *IEEE Trans. Power Electron.*, vol. 27, no. 8, pp. 3817–3825, Aug. 2012.
[7] M. Jansson, L. Harnefors, O. Wallmark, and M. Leksell, "Synchronization at startup and stable rotation reversal of sensorless nonsalient PMSM drives," *IEEE Trans. Ind. Electron.*, vol. 53, no. 2, pp. 379–387, Apr. 2006.
[8] S. Tsotoulidis and A. N. Safacas, "Deployment of an adaptable sensorless commutation technique on BLDC motor drives exploiting zero sequence voltage," *IEEE Trans. Ind. Electron.*, vol. 62, no. 2, pp. 877–886, Feb. 2015.
[9] M. Tursini, R. Petrella, and F. Parasiliti, "Initial rotor position estimation method for PM motors," *IEEE Trans. Ind. Appl.*, vol. 39, no. 6, pp. 1630–1640, Nov. 2003.
[10] N. Bianchi, E. Fornasiero, and S. Bolognani, "Effect of stator and rotor saturation on sensorless rotor position detection," *IEEE Trans. Ind. Appl.*, vol. 49, no. 3, pp. 1333–1342, May 2013.
[11] M. Boussak, "Implementation and experimental investigation of sensorless speed control with initial rotor position estimation for interior permanent magnet synchronous motor drive," *IEEE Trans. Power Electron.*, vol. 20, no. 6, pp. 1413–1422, Nov. 2005.
[12] P. L. Jansen and R. D. Lorenz, "Transducerless position and velocity estimation in induction and salient AC machines," *IEEE Trans. Ind. Appl.*, vol. 31, no. 2, pp. 240–247, Mar. 1995.
[13] J.-I. Ha and S.-K. Sul, "Sensorless field-orientation control of an induction machine by high-frequency signal injection," *IEEE Trans. Ind. Appl.*, vol. 35, no. 1, pp. 45–51, Jan. 1999.
[14] H. W. D. Kock, M. J. Kamper, and R. M. Kennel, "Anisotropy comparison of reluctance and PM synchronous machines for position sensorless control using HF carrier injection," *IEEE Trans. Power Electron.*, vol. 24, no. 8, pp. 1905–1913, Aug. 2009.
[15] H. A. Toliyat, L. Hao, D. S. Shet, and T. A. Nondahl, "Position-sensorless control of surface-mount permanent-magnet AC (PMAC) motors at low speeds," *IEEE Trans. Ind. Electron.*, vol. 49, no. 1, pp. 157–164, Feb. 2002.

[16] Y.-S. Jeong, R. D. Lorenz, T. M. Jahns, and S.-K. Sul, "Initial rotor position estimation of an interior permanent-magnet synchronous machine using carrier-frequency injection methods," *IEEE Trans. Ind. Appl.*, vol. 41, no. 1, pp. 38–45, Jan. 2005.
[17] D. Raca, P. Garcia, D. D. Reigosa, F. Briz, and R. D. Lorenz, "Carrier-signal selection for sensorless control of PM synchronous machines at zero and very low speeds," *IEEE Trans. Ind. Appl.*, vol. 46, no. 1, pp. 167–178, Jan. 2010.
[18] T. Noguchi, K. Yamada, S. Kondo, and I. Takahashi, "Initial rotor position estimation method of sensorless PM synchronous motor with no sensitivity to armature resistance," *IEEE Trans. Ind. Electron.*, vol. 45, no. 1, pp. 118–125, Feb. 1998.
[19] H. Kim, K.-K. Huh, R. D. Lorenz, and T. M. Jahns, "A novel method for initial rotor position estimation for IPM synchronous machine drives," *IEEE Trans. Ind. Appl.*, vol. 40, no. 5, pp. 1369–1378, Sep. 2004.
[20] R. Antonello, F. Tinazzi, and M. Zigliotto, "Benefits of direct phase voltage measurement in the rotor initial position detection for permanent-magnet motor drives," *IEEE Trans. Ind. Electron.*, vol. 62, no. 11, pp. 6719–6726, Nov. 2015.
[21] W.-J. Lee and S.-K. Sul, "A new starting method of BLDC motors without position sensor," *IEEE Trans. Ind. Appl.*, vol. 42, no. 6, pp. 1532–1538, Nov./Dec. 2006.
[22] S. Nakashima, Y. Inagaki, and I. Miki, "Sensorless initial rotor position estimation of surface permanent-magnet synchronous motor," *IEEE Trans. Ind. Appl.*, vol. 36, no. 6, pp. 1598–1603, Nov. 2000.
[23] C. L. Baratieri and H. Pinheiro, "A novel starting method for sensorless brushless DC motors with current limitation," in *Proc. 20th Int. Conf. Elect. Mach.*, Sep. 2012, pp. 816–822.
[24] F. Gabriel, F. De Belie, X. Neyt, and P. Lataire, "High-frequency issues using rotating voltage injections intended for position self-sensing," *IEEE Trans. Ind. Electron.*, vol. 60, no. 12, pp. 5447–5457, Dec. 2013.
[25] X. Luo, Q. Tang, A. Shen, and Q. Zhang, "PMSM sensorless control by injecting HF pulsating carrier signal into estimated fixed-frequency rotating reference frame," *IEEE Trans. Ind. Electron.*, vol. 63, no. 4, pp. 2294–2303, Apr. 2016.
[26] S. Ogasawara and H. Akagi, "Implementation and position control performance of a position-sensorless IPM motor drive system based on magnetic saliency," *IEEE Trans. Ind. Appl.*, vol. 34, no. 4, pp. 806–812, Jul. 1998.
[27] C. Silva, G. M. Asher, and M. Sumner, "Hybrid rotor position observer for wide speed-range sensorless PM motor drives including zero speed," *IEEE Trans. Ind. Electron.*, vol. 53, no. 2, pp. 373–378, Apr. 2006.
[28] S. Murakami, T. Shiota, M. Ohto, K. Ide, and M. Hisatsune, "Encoderless servo drive with adequately designed IPMSM for pulse-voltage-injection-based position detection," *IEEE Trans. Ind. Appl.*, vol. 48, no. 6, pp. 1922–1930, Nov./Dec. 2012.
[29] J. Liu, T. Matsuo, T. A. Nondahl, P. B. Schmidt, T. M. Rowan, and R. J. De Lange, "Implementation and performance of position sensorless PMSM control in industrial drives," in *Proc. IEEE Ind. Appl. Soc. Annu. Meeting*, Oct. 2014, pp. 1–8.
[30] M. Pacas, "Sensorless drives in industrial applications," *IEEE Ind. Electron. Mag.*, vol. 5, no. 2, pp. 16–23, Jun. 2011.
[31] D. Raca, M. C. Harke, and R. D. Lorenz, "Robust magnet polarity estimation for initialization of PM synchronous machines with near-zero saliency," *IEEE Trans. Ind. Appl.*, vol. 44, no. 4, pp. 1199–1209, Jul. 2008.
[32] P. L. Xu and Z. Q. Zhu, "Novel carrier signal injection method using zero-sequence voltage for sensorless control of PMSM drives," *IEEE Trans. Ind. Electron.*, vol. 63, no. 4, pp. 2053–2061, Apr. 2016.
[33] J. Hu, J. Liu, and L. Xu, "Eddy current effects on rotor position estimation and magnetic pole identification of PMSM at zero and low speeds," *IEEE Trans. Power Electron.*, vol. 23, no. 5, pp. 2565–2575, Sep. 2008.
[34] L. M. Gong and Z. Q. Zhu, "Robust initial rotor position estimation of permanent-magnet brushless AC machines with carrier-signal-injection-based sensorless control," *IEEE Trans. Ind. Appl.*, vol. 49, no. 6, pp. 2602–2609, Nov./Dec. 2013.
[35] J.-I. Ha, K. Ide, T. Sawa, and S.-K. Sul, "Sensorless rotor position estimation of an interior permanent-magnet motor from initial states," *IEEE Trans. Ind. Appl.*, vol. 39, no. 3, pp. 761–767, May 2003.
[36] Y.-D. Yoon, S.-K. Sul, S. Morimoto, and K. Ide, "High-bandwidth sensorless algorithm for AC machines based on square-wave-type voltage injection," *IEEE Trans. Ind. Appl.*, vol. 47, no. 3, pp. 1361–1370, May/Jun. 2011.
[37] D. Nguyen, R. Dutta, M. F. Rahman, and J. E. Fletcher, "Performance of a sensorless controlled concentrated-wound interior permanent-magnet synchronous machine at low and zero speed," *IEEE Trans. Ind. Electron.*, vol. 63, no. 4, pp. 2016–2026, Apr. 2016.

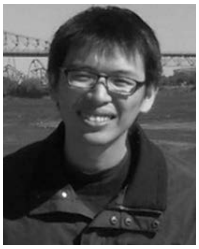

**SHIH-CHIN YANG** (S'10–M'12) was born in Taiwan. He received the M.S. degree in mechanical engineering from National Taiwan University, Taiwan, and the Ph.D. degree in mechanical engineering from the University of Wisconsin–Madison, WI, USA, in 2007 and 2011. From 2011 to 2015, he was a Research Engineer with the Texas Instruments Motor Laboratory, Dallas, TX, USA. He is currently an Assistant Professor with National Taiwan University, Taiwan, with the responsibility on the development of motor drive and motor control technology. His research interests include motor drive, power electronics, and control systems. He was a recipient of the IEEE Industry Applications Society Industrial Drive Committee First Prize Paper Award in 2011.

**SHENG-MING YANG** (M'90) received the M.S. and Ph.D. degrees from the University of Wisconsin–Madison in 1985 and 1989, respectively. From 1989 to 1992, he was a Development Engineer with Unico Inc., and from 1992 to 1995, he was a Principal Engineer with the Corporate Technology Center, A. O. Smith Co., Milwaukee, WI, USA. In 1995, he joined the Department of Mechanical and Electro-Mechanical Engineering, Tamkang University, Taiwan, as a Professor. Since 2007, he joined the Department of Electrical Engineering, National Taipei University of Technology, Taiwan. His research interests are ac and dc motor drives and control.

**JING-HUI HU** was born in Taipei, Taiwan, in 1992. He received the M.S. degree from the National Taipei University of Technology, Taiwan, in 2016. He is currently with the Industrial Technology Research Institute, Hsinchu, Taiwan. His research interests include ac motor drives and control.